


ORIGINAL ARTICLE

Open Access



Strain and stress conditions at crack initiation during shearing of medium- and high-strength steel sheet

E. Gustafsson^{1*} , S. Marth², L. Karlsson¹ and M. Oldenburg²

Abstract

Background: Strain and stress conditions in sheet metal shearing are of interest for calibration of various fracture criteria. Most fracture criteria are governed by effective strain and stress triaxiality.

Methods: This work is an attempt to extend previous measurements of strain fields in shearing of steel sheets with the stress state calculated from the measured displacement fields. Results are presented in terms of von Mises stress and stress triaxiality fields, and a comparison was made with finite element simulations. Also, an evaluation of the similarities of the stress conditions on the sheet surface and inside the bulk material was presented.

Results: Strains and von Mises stresses were similar to the surface and the bulk material, but the stress triaxiality was not comparable. There were large gradients in strain and stress around the curved tool profiles that made the result resolution dependent and comparisons of maximum strain and stress values difficult.

Conclusions: The stress state on the sheet surface calculated from displacement field measurements is useful for validation of a three-dimensional finite element model.

Keywords: Sheet metal, Experiment, Shearing, Strain, Stress, Crack initiation

Background

Shearing is a common process in the sheet metal industry. The constant development of new sheet materials with various shearing properties makes it desirable to have a model of the shearing process that can predict the appropriate shearing parameters. That model must consider the fracture in addition to the large plastic deformations. Numerous fracture criteria, based on strain and stress conditions, exist which can be used in finite element (FE) models of the shearing, for example, maximum effective strain, maximum shear stress, or combined stress and strain criteria (Cockcroft and Latham 1968; Johnson and Cook 1985). Such criteria need to be calibrated against experimentally measured strain and stress conditions. The ductile fracture is in general governed by effective strain and stress triaxiality as observed by McClintock (1968). Low triaxiality results in shear dimple rupture whereas

high triaxiality results in void coalescence as modelled by Rice and Tracey (1969).

Strain and stress conditions can be calculated from full-field measurements of displacement as shown by Marth et al. (2016). In that work, incremental displacement fields were obtained from captured images during the experiments by the digital image correlation (DIC) technique, thorough reviewed by Hild and Roux (2006). With DIC, the displacements are measured on sub-pixel level, see for example Sjödaahl (1994). Accuracy in DIC measurements are covered in detail by Sjödaahl (1997).

Strains were measured during planar blanking by Stegeman et al. (1999) and in experiments with a symmetric shearing set-up by Gustafsson et al. (2016b). The purpose of the present work was to extend these experiments with stress calculations using the method described by Marth et al. (2016), to determine the strain and stress conditions at crack initiation. The calculated stresses were compared with stresses from FE simulations at the stage of crack initiation.

*Correspondence: egu@du.se

¹Dalarna University, SE-791 88 Falun, Sweden

Full list of author information is available at the end of the article

Methods

Materials and yield stress model

The medium-strength (MS) construction steel SSAB Domex 420 MC, and the high-strength (HS) wear plate steel SSAB Hardox 400, with mechanical properties according to Table 1, were used in the study. The yield stress for the sheet materials was described with the exponential hardening law suggested by Hollomon (1945), $\sigma_Y = K\bar{\epsilon}_p^n$, where $\bar{\epsilon}_p$ is the effective plastic strain and K and n are material specific parameters. These parameters were fitted to compression test data provided by Gustafsson et al. (2016b) and are shown in Table 1 for the sheared material grades.

Shearing experiment

The shearing experiments were performed with the method and set-up developed by Gustafsson et al. (2014). This set-up uses symmetry to balance the force defined as F_x in Fig. 1. Therefore, no guides with friction losses are needed, and the forces, F_x and F_y , which are measured in the set-up, are accurate. The design also features large stiffness in the x -direction and thus a stable tool clearance c . Tool displacements, U_x and U_y , were measured with linear transducers as described by Gustafsson et al. (2016a). Tool clearance and clamping of the sheet samples were varied in the experiments: clearances $0.05h$, $0.15h$ and $0.25h$, where h is the sheet thickness used and the sheet was clamped on one or both sides as shown in Fig. 1.

Images of the approximately magnified area shown in Fig. 1 were captured during the shearing to register the in-plane deformation of the sheet. For this purpose, the xy -surface of the sheet samples was prepared with a random speckle pattern for subsequent digital image correlation. Further details on the experiments are described by Gustafsson et al. (2016b).

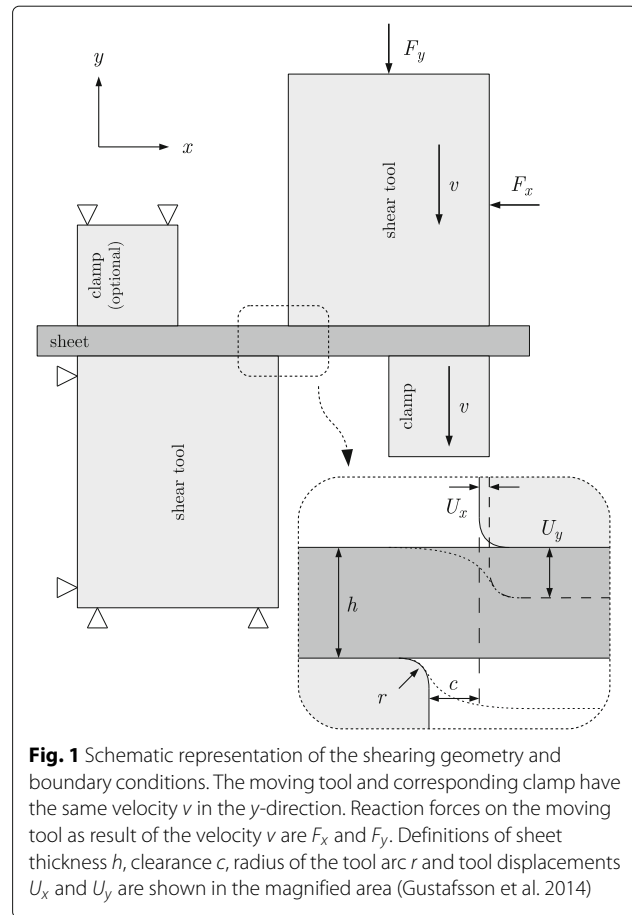
Image analysis and strain evaluation

The digital image correlation (DIC) technique, implemented with the commercial software ARAMIS, was used to calculate the deformation gradients on the surface. The evaluated area was partitioned into sub-areas, called facets, and then, these facets were traced

Table 1 Mechanical properties in terms of yield strength Rp02, tensile strength Rm and elongation A80, evaluated from uniaxial tensile tests of sheet metal grades used in the study

Material strength	Rp02 [MPa]	Rm [MPa]	A80 [%]	h [mm]	K [MPa]	n [—]
Medium	450	520	25	5.97–6.03	880	0.127
High	1080	1260	7	6.11–6.15	1550	0.0345

The range of sheet thickness h for the sheared samples is also shown. Finally, K and n are the hardening law parameters for the two material grades as fitted to compression test data

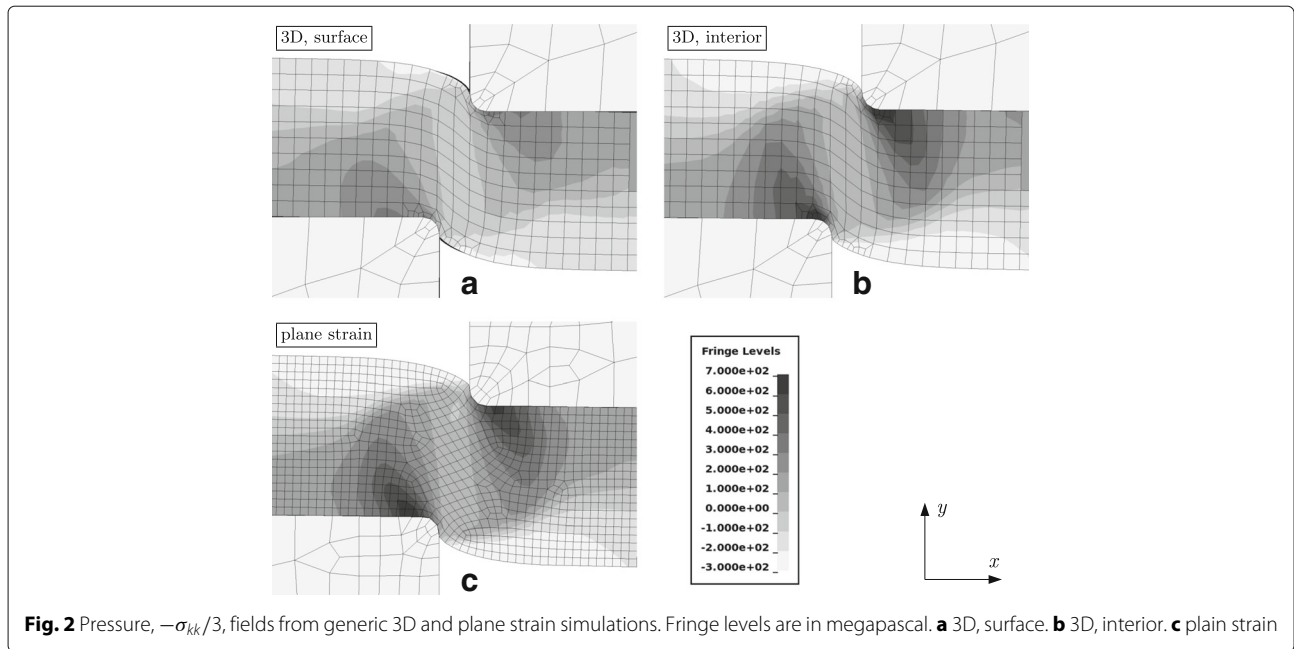


through cross-correlation of the images captured during the shearing. The facet size was 64×64 pixels, and the facet step size was 8 pixels in each direction. The in-plane strain field (x - and y -components) was calculated from the measured deformations, and under assumption of plastic incompressibility, the missing strain component (z -direction) was calculated, as shown by Kajberg and Lindkvist (2004).

Evaluation of stress from measured strain

The strain tensor, obtained as described in previous subsection, was used to calculate the stress tensor by a radial return algorithm based on isotropic von Mises plasticity, as described by Marth et al. (2016), but without using a stepwise modelling of the hardening relation. Instead of this stepwise modelling, the plastic work hardening of the materials was modelled with the Hollomon hardening law using the material parameter presented in Table 1. From the stress tensor, the effective von Mises stress was calculated as

$$\bar{\sigma} = \sqrt{\frac{3}{2} s_{ij} s_{ij}}, \quad (1)$$



where $s_{ij} = \sigma_{ij} - \sigma_{kk}\delta_{ij}/3$ is the deviatoric stress tensor. Taking the mean stress, $\sigma_m = \sigma_{kk}/3$, the stress triaxiality state can be calculated as

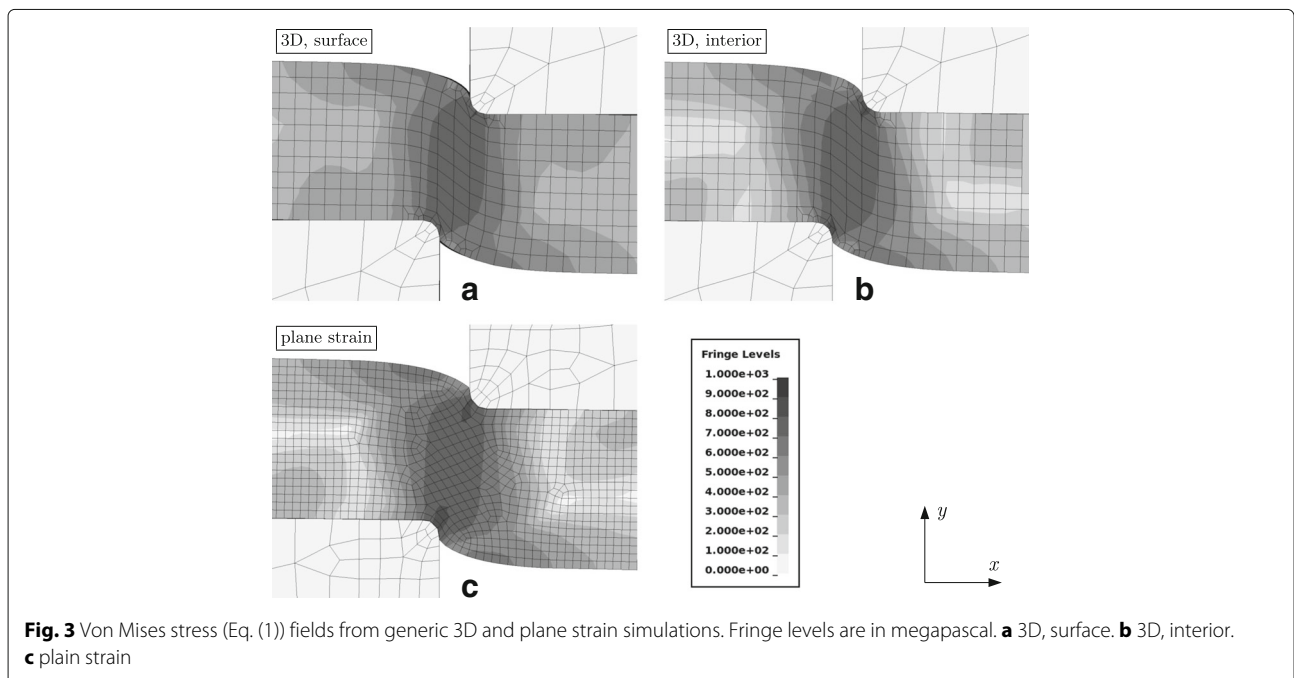
$$\eta = \frac{\sigma_m}{\bar{\sigma}} \tag{2}$$

Since the strain values used in this method were obtained on the material surface, a plane stress approach was used to evaluate the surface stress conditions. A

plane strain approach would otherwise be the intuitive choice to analyse the stress state inside the material, but that approach would violate the plastic incompressibility condition.

Finite element simulations

Plane strain FE analyses of the shearing were performed with a commercial general-purpose finite element software. Geometry and boundary conditions for the model



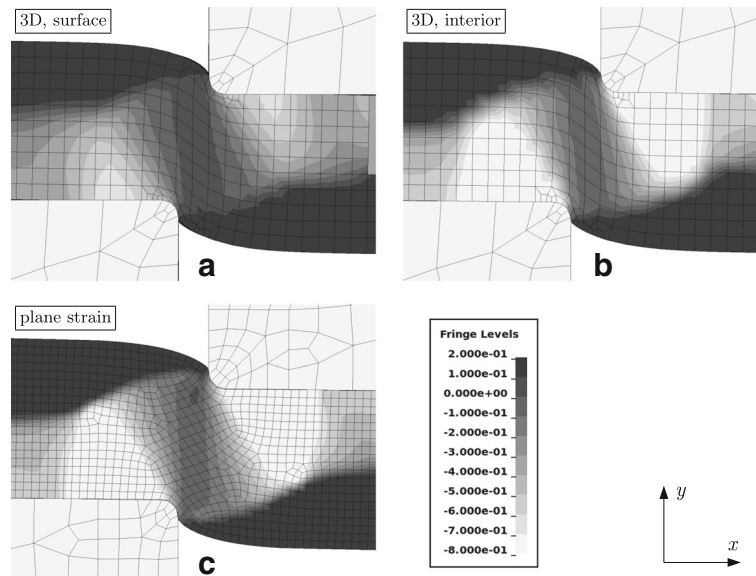


Fig. 4 Stress triaxiality (Eq. (2)) fields from generic 3D and plane strain simulations. **a** 3D, surface. **b** 3D, interior. **c** plain strain

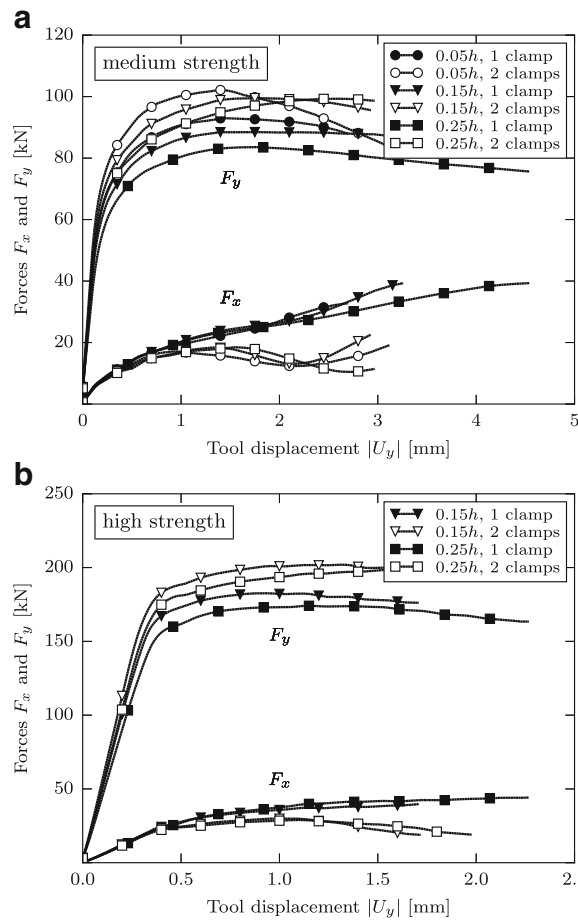


Fig. 5 FE simulated force-displacement curves when shearing the medium-strength material (**a**) and the high-strength material (**b**). Clearances (expressed as fractions of sheet thickness h) and clamping configurations are indicated in the figure legend

are described in detail by Gustafsson et al. (2014). The model was coarsely meshed except in the area where large deformations were expected and a denser mesh was required to resolve gradients in the state variables. The undeformed element size in the dense area was 0.1 mm. Four-noded and fully integrated plane strain elements were used for sheet and tools. Adaptive remeshing was applied to avoid large aspect ratios of the elements. Contacts were modelled with surface to surface formulations, and both static and dynamic friction coefficients were 0.1.

A model with elastic tools and an isotropic elastic-plastic sheet material, where Poisson’s ratio was 0.3 and Young’s modulus was 210 GPa, was used. A constant tool acceleration of 100 mm s⁻² was used in all simulations. This is a rough approximation of the experimental conditions, but still satisfactory since no rate or temperature effects were modelled.

For a preliminary study of the stress state on the sheet surface and in the interior of the material, generic FE models were used in three dimensions (3D) and in plane strain. For this purpose, a slightly different geometry, material parameters and, most notably, no remeshing were applied in the 3D model. This 3D model was therefore only useful at relatively small tool displacements.

Comparison between experiments and simulations

Comparisons were made between results from FE simulations and results based on measurements, in terms of effective von Mises stress (Eq. (1)) and stress triaxiality (Eq. (2)). Furthermore, effective strain and tool forces versus tool displacement were presented for comparison with corresponding experimental data presented by Gustafsson et al. (2016b). An agreement between these simulations and experiments (effective strain and force vs. displacement) should be seen as a validation of the FE model. The effective plastic strain fields from the FE simulations

$$\bar{\epsilon}_p = \int \sqrt{\frac{2}{3} D_{ij}^p D_{ij}^p} dt, \tag{3}$$

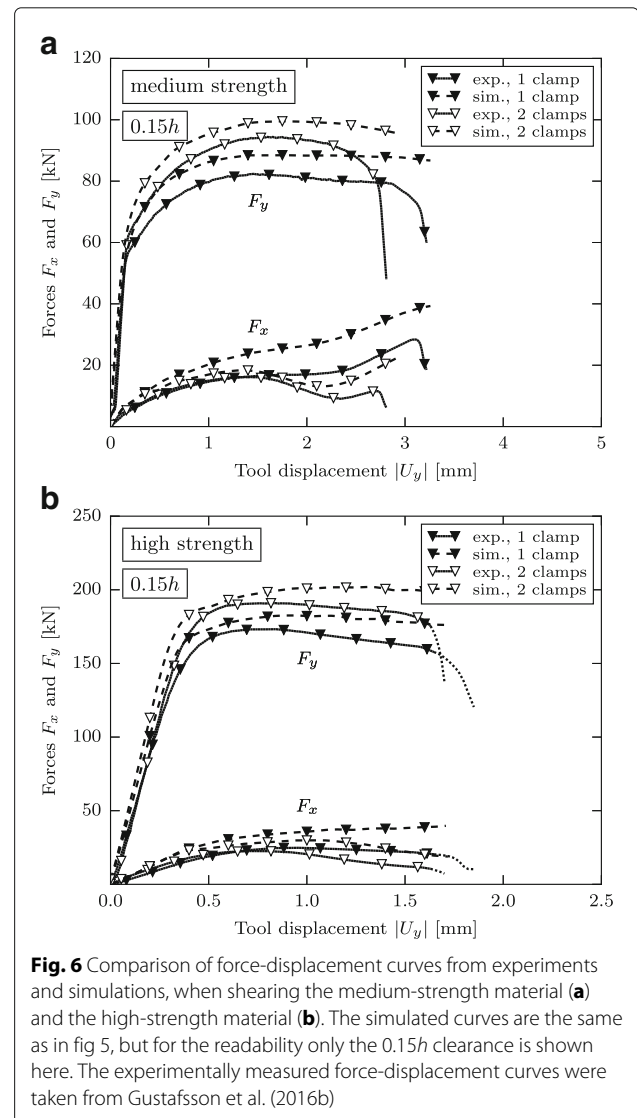
where D_{ij}^p is the plastic component of the rate of deformation tensor, which can be compared with the effective strains measured by Gustafsson et al. (2016b), since the elastic part of the latter is negligible.

All presented strains and stresses are from the stage of crack initiation. The fracture was not modelled in the FE simulations, and a comparison with experiments is therefore irrelevant after crack initiation.

Results

First, results from generic FE simulations are presented to show how the stress state varies between the surface and the bulk material, and that plane strain is a satisfactory

approximation of the conditions in the bulk material (“Generic FE simulations of the stress state” section). Second, the FE model of the experimental shearing conditions is validated against previously published tool forces and strain fields (“Validation of the FE model at experimental conditions” section). Third, a comparison between the stress state from FE simulations and from calculations based on the measured displacement fields is presented, in terms of effective von Mises stress (“Comparison of von Mises stress” section) and stress triaxiality (“Comparison of stress triaxiality” section). The stress calculated from measured displacement fields will hereafter be referred to as experimental stress. Finally, a summary of the comparison between simulated and experimentally based stress and strain conditions closes this section (“Summary of measured and simulated results” section).



Generic FE simulations of the stress state

Strains on the sheet surface and inside the sheet are almost the same during shearing, as showed by Gustafsson et al. 2016b. Here, the same 3D and plane strain FE models were used to investigate the stress state in terms of mean stress (pressure), von Mises stress and triaxiality. Results from the generic FE simulations are presented in Figs. 2, 3 and 4. Plane strain was a good approximation of the interior stress state according to the evaluated parameters (Figs. 2b–c, 3b–c and 4b–c), but the surface stress, in terms of pressure and triaxiality, was not comparable to the stress in the bulk material (Figs. 2a–b and 5a–b).

There was, however, a good agreement between the von Mises stress on the surface and the interior (Fig. 3a–b). This was expected since the effective strain was in good agreement between surface and the interior in a previous

comparison by Gustafsson et al. (2016b). The von Mises stress gradients were largest outside of the plastic zone. This was also expected since the gradient, after the yield locus is reached, is proportional to the hardening modulus which is much smaller than the Young’s modulus.

In the area between the arcs of the tools, the pressure was lower on the surface compared to the interior and the triaxiality was larger. The triaxiality in the material between the tools was in general slightly positive on the surface and slightly negative in the bulk material at this state of the shearing.

Validation of the FE model at experimental conditions

Tool forces from the FE simulations, up to the tool displacement $|U_y|$ where final fracture occurred in the experiments, are presented in Fig. 5. All trends in the

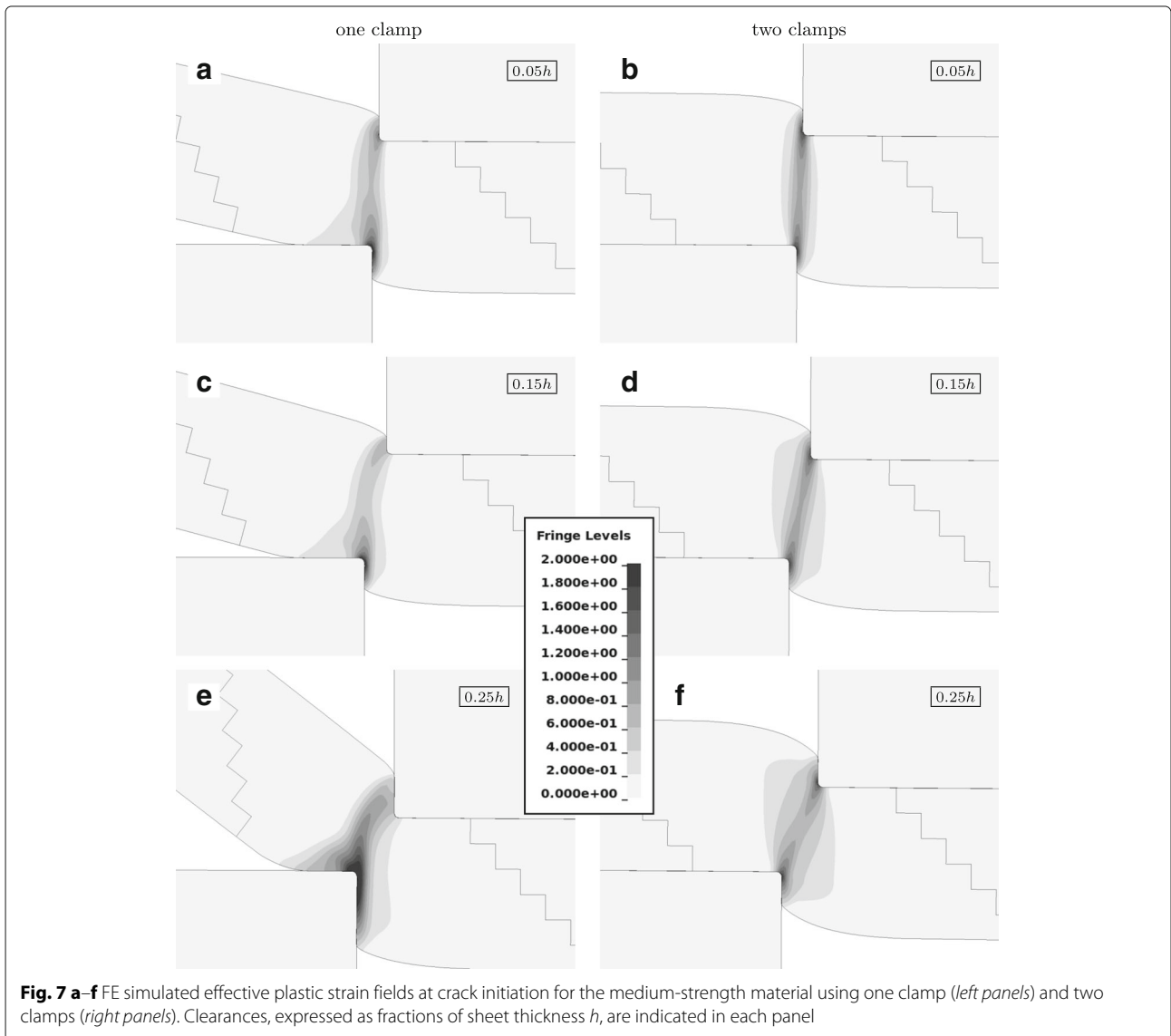


Fig. 7 a–f FE simulated effective plastic strain fields at crack initiation for the medium-strength material using one clamp (left panels) and two clamps (right panels). Clearances, expressed as fractions of sheet thickness h , are indicated in each panel

forces from variations of the tool clearance and clamping configurations, and the general shape of the force curves, were the same in the simulations shown here as in the experiments by Gustafsson et al. (2016b). There was, however, a slight overestimation of both force components F_x and F_y in the simulations, as shown in Fig. 6. In general, the overestimation increased along with the tool displacement, $|U_y|$, for both materials, but for the medium-strength material, the overestimation in F_y was almost constant. The drop in forces after crack initiation, seen in the experiments, was not captured by the simulations since crack formation was not accounted for in the model.

Effective plastic strains from FE simulations for the two material grades at the stage of crack initiation are shown in Figs. 7 and 8. There was a good agreement between the experiments presented by Gustafsson et al. (2016b) and the simulations shown here. The large gradients close to the arc of the tool were better resolved in the simulations, and a comparison of the largest strains was therefore not straightforward.

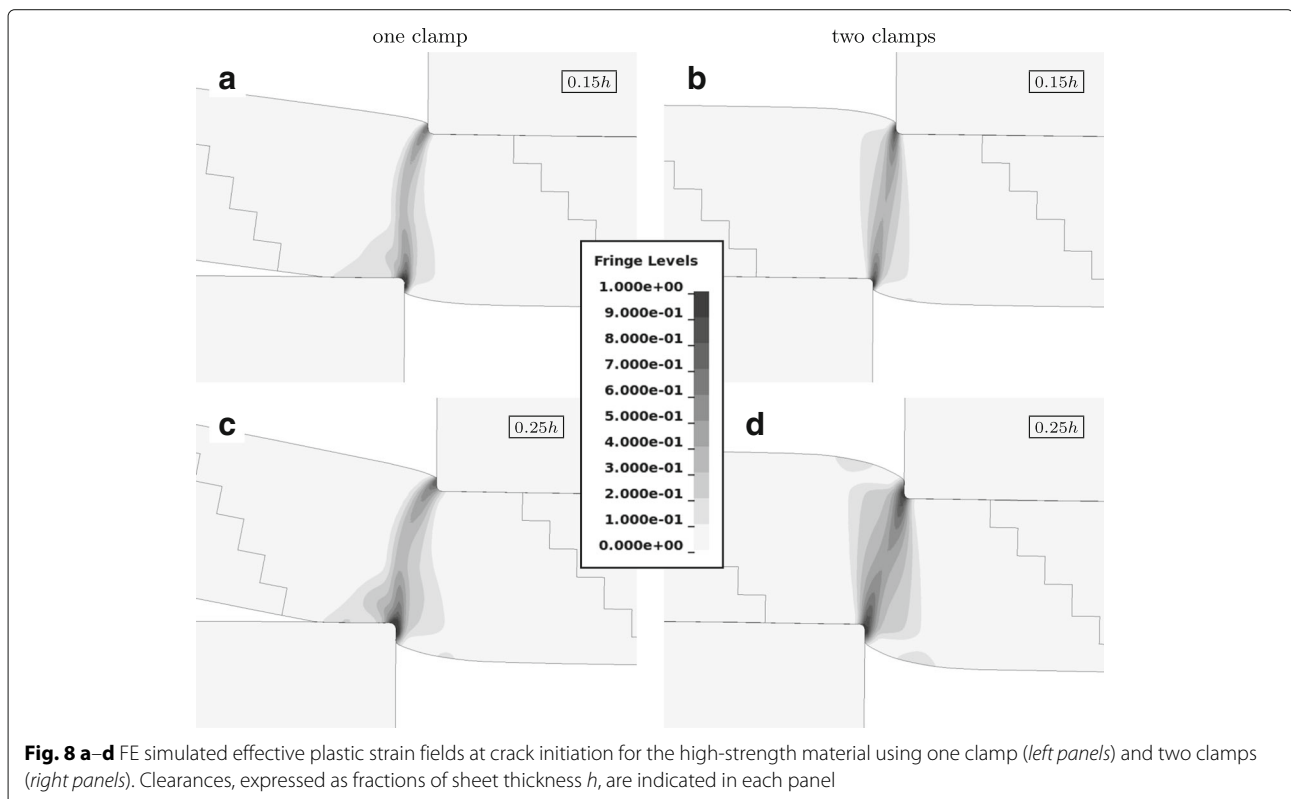
Comparison of von Mises stress

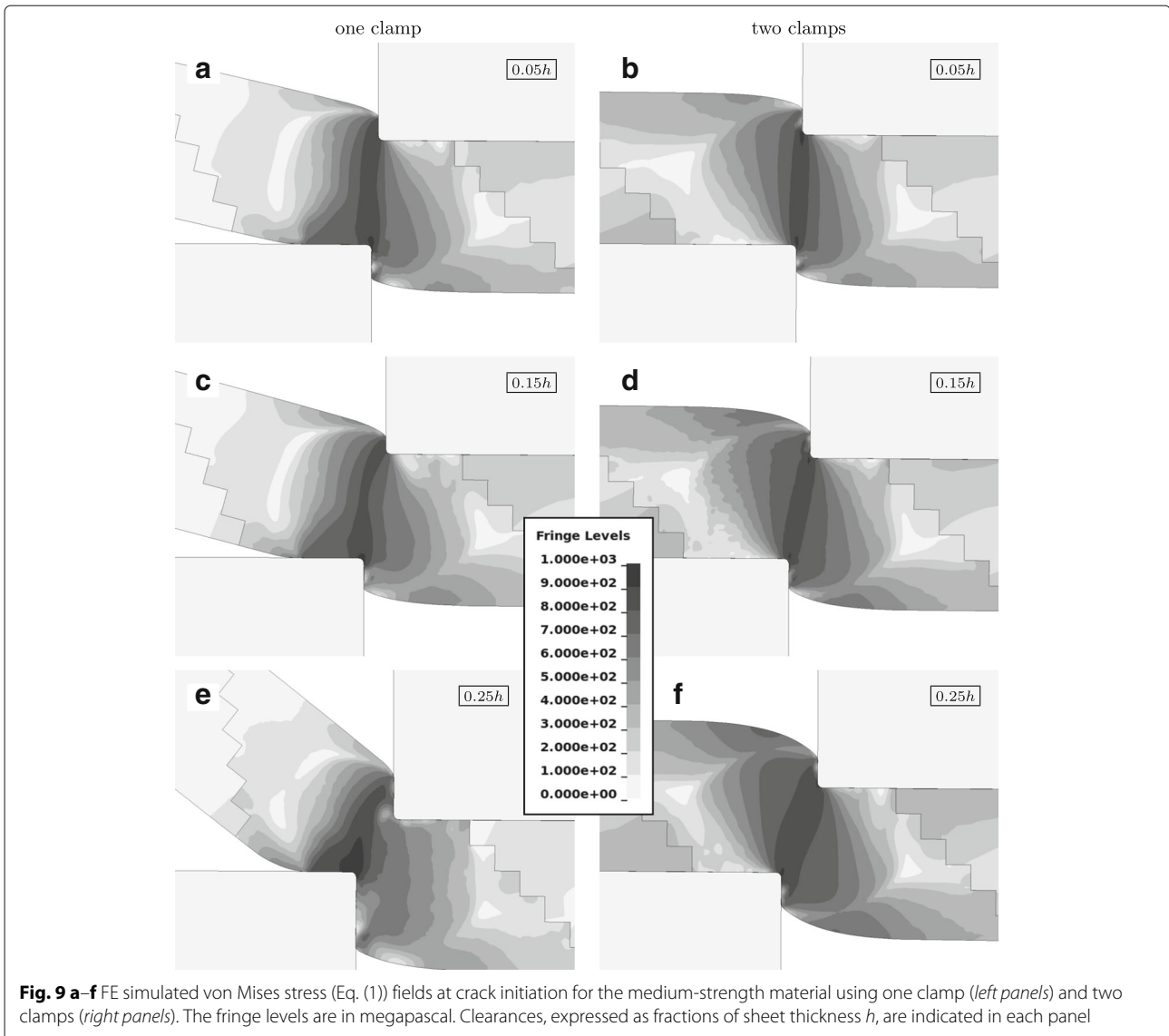
Von Mises stresses from FE simulations are presented in Figs. 9 and 11, and the corresponding experimental stresses are presented in Figs. 10 and 12. As for the strains, there was a good agreement between the von

Mises stresses from FE simulations and experiments. The experimental results showed less details compared with the simulations, especially at the sheet edges. Missing information at the edges also resulted in a shape of the imaged area without a distinct indentation of the tools into the sheet (Figs. 10 and 12). For some experiments, white areas of missing data extends further into the sheet from the edge. This is most pronounced in Fig. 10e, where the deformations were largest.

Comparison of stress triaxiality

Stress triaxiality from FE simulations are shown in Figs. 13 and 15 and from experiments in Figs. 14 and 16. The calculated triaxialities contained much noise, especially in areas with small von Mises stresses due to the definition as the ratio of mean stress to von Mises stress. Therefore, the data in Figs. 14 and 16 was low-pass filtered to improve the readability. In general, the triaxiality was larger in the area close to the vertical surface of the tools next to the arc of the tool than in an area close to the arc itself. The areas of the largest triaxiality, along the horizontal sheet edge that is not in contact with the tool, were not subject to notable effective strains, and therefore, no cracks were observed there. Since the simulations (Figs. 13 and 15) show the stress state in the bulk material and the experiments (Figs. 14 and 16) show the stress state on the surface, these triaxiality fields were not comparable.



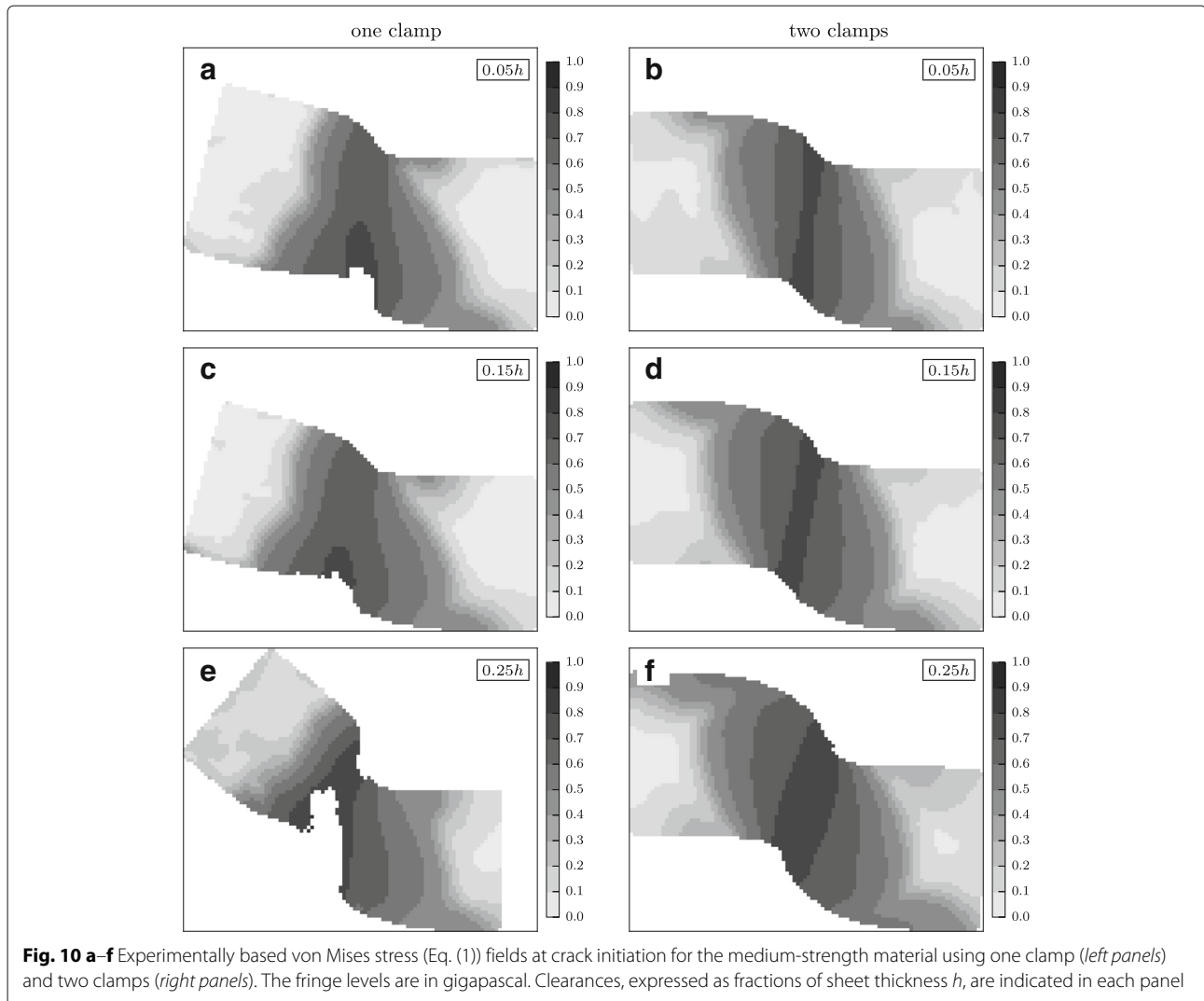


Summary of measured and simulated results

In addition to the fringe plots of stress and strain presented (Figs. 7, 8, 9, 10, 11, 12, 13, 14, 15 and 16), a numeric summary of these parameters, at crack initiation, is provided in Table 2. The parameters were evaluated in three regions of the sheet in the vicinity of the arc-shaped 2D profile of the lower tool, as indicated in Fig. 17. At point I, where the curvature of the tool profile changes, the material is heavily loaded and large stresses and strains are therefore expected there. Large strain gradients from the simulated data were found close to the tool; hence, point II was chosen a short distance away from the curved tool profile. There were large stress triaxialities in the simulated data in region III, where the sheet is in contact with the vertical tool profile just

below point I. Moreover, cracks were sometimes found in this region.

The summary in Table 2 shows that strains at point I were larger in the simulations, $\bar{\epsilon}_I^{\text{sim}}$, than in the experiments, $\bar{\epsilon}_I^{\text{exp}}$. The simulations indicated a large strain gradient between points I and II, but such gradient could not be revealed from the experiments since points I and II could not be distinguished due to the experimental resolution. There was a reasonable agreement between the simulated and experimentally based von Mises stresses for the high-strength material; the agreement was less satisfactory for the medium-strength material. There was no clear trend of stress triaxiality for either material strength, tool clearance or clamping configuration, but there was still a large spread of measured values.



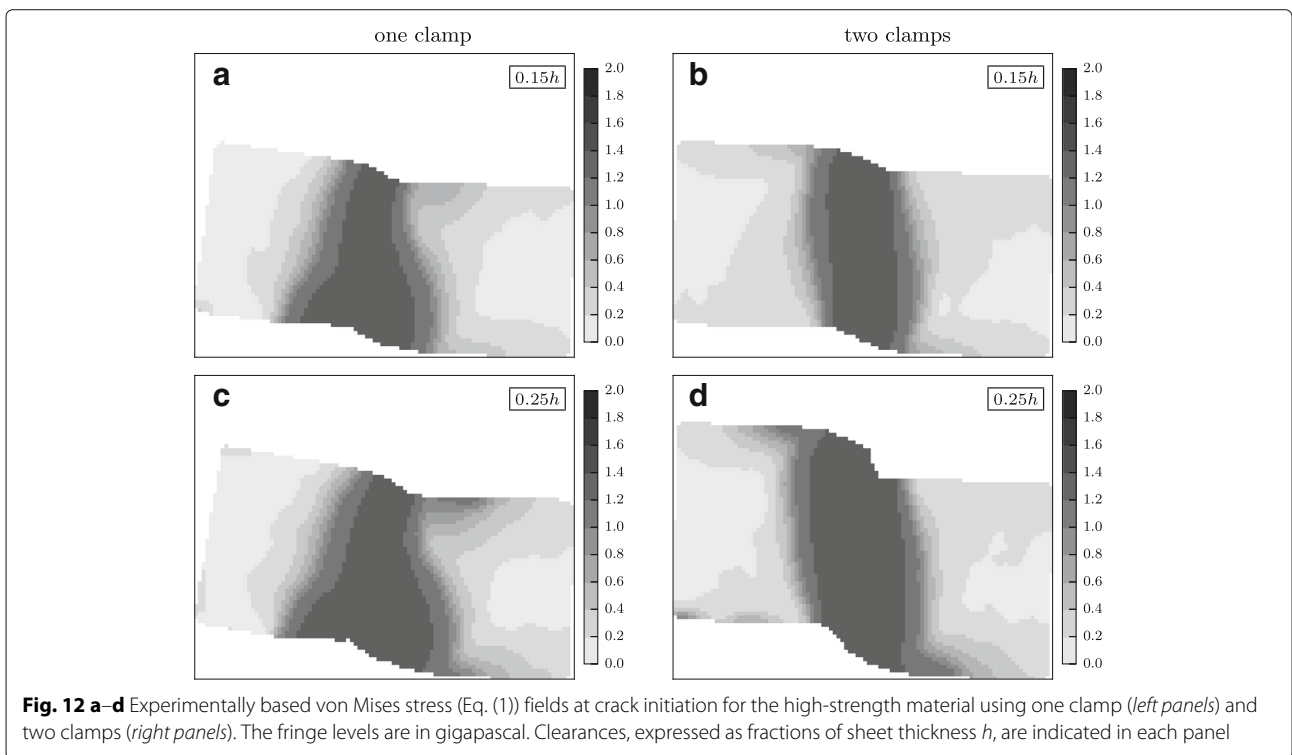
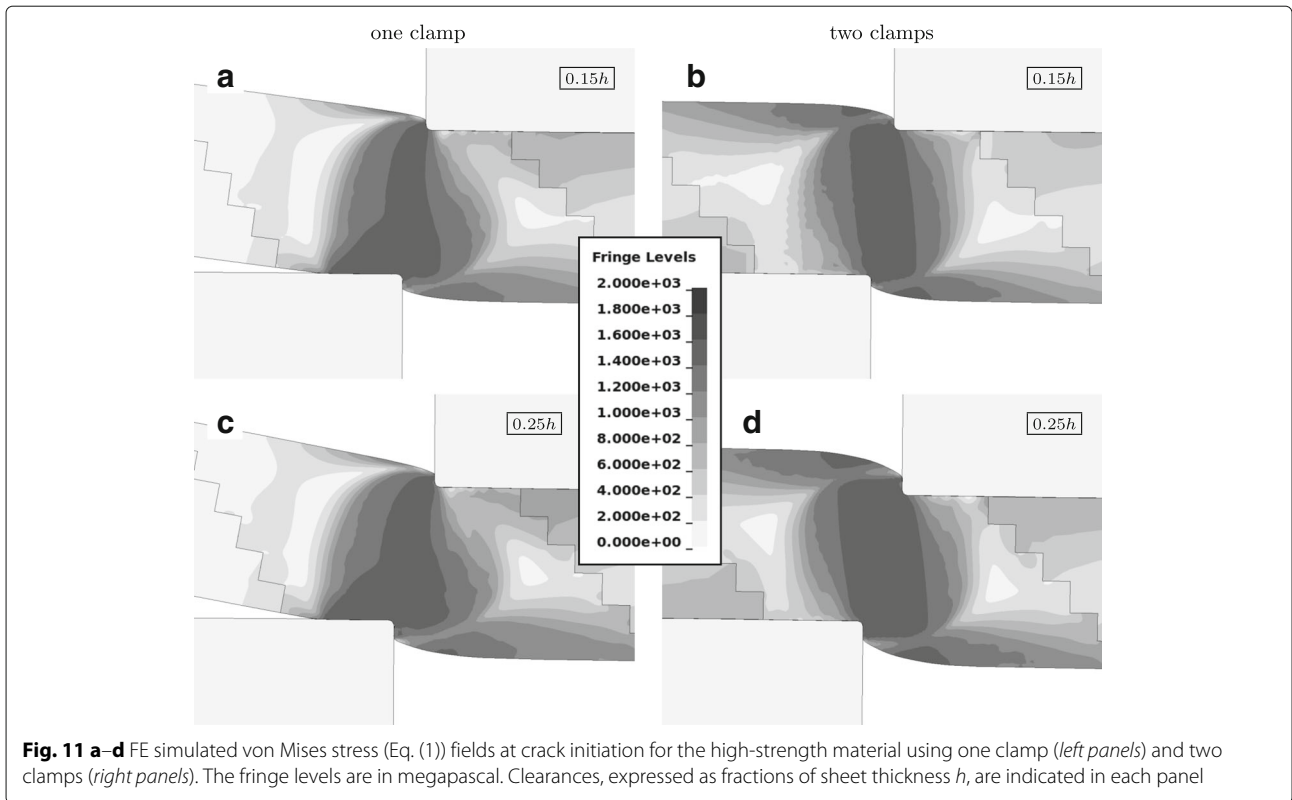
Discussion

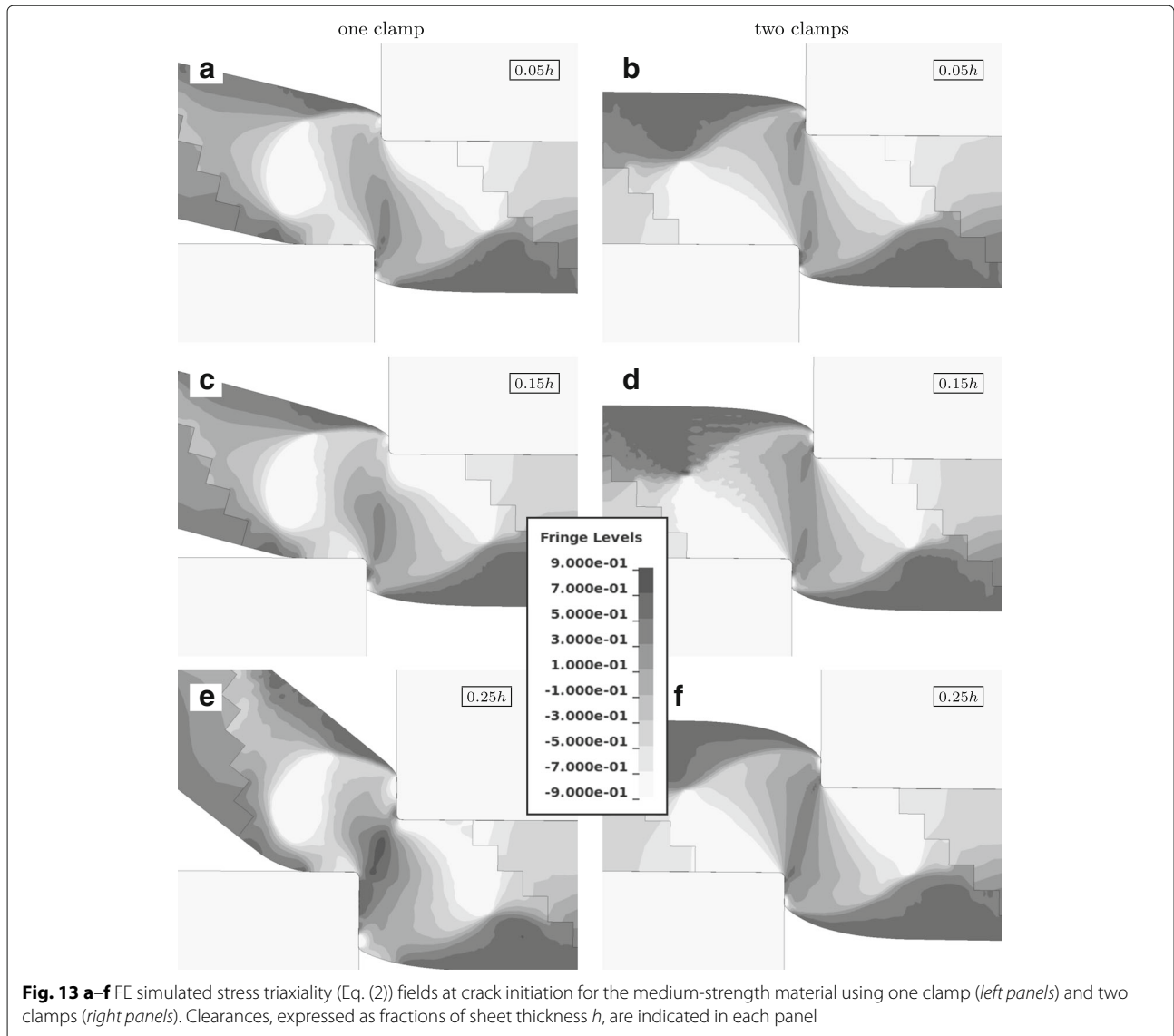
Tool forces were slightly overestimated by the applied FE model already from small tool displacements, as shown in Fig. 6. Possible reasons include an incorrect material yield strength and hardening and also the friction coefficient between sheet and tools. The materials were characterised by accurate compression tests, but only data from the thickness direction were used for the isotropic model and there was no perfect fit of the exponential hardening law to the compression test data. The friction coefficient was studied in the sensitivity analyses by Gustafsson et al. (2014) and had large effects on the tool forces. An increased friction coefficient resulted in largely increased F_x and increased F_y along with the tool displacement.

The large strain gradients in the sheet material around the curved tool profile made the comparison between measurements and simulations difficult, as the results were resolution dependent. These gradients, expressed

as relative increase of strain from point II to point I (a distance of about 0.2 mm), varied from 26% to almost 90%, depending on shearing configuration and material strength. There was also a limitation in the measurement technique that prevented accurate measurements close to the edges as discussed by Gustafsson et al. (2016b). Also, due to the same phenomenon, measured strains after crack initiation would likely be overestimated since the image correlation algorithm and strain calculations interpret relative movement of the fractured parts as strain.

The comparison of the stress state between experiments and simulations is problematic since the calculations based on the measured strain give the stress state on the surface and the simulations in plane strain give the stress state in the bulk material. The obtained von Mises stress was still almost identical between the two methods, but the triaxiality differed in both distribution and levels. Possibly, the triaxiality from both methods are correct,

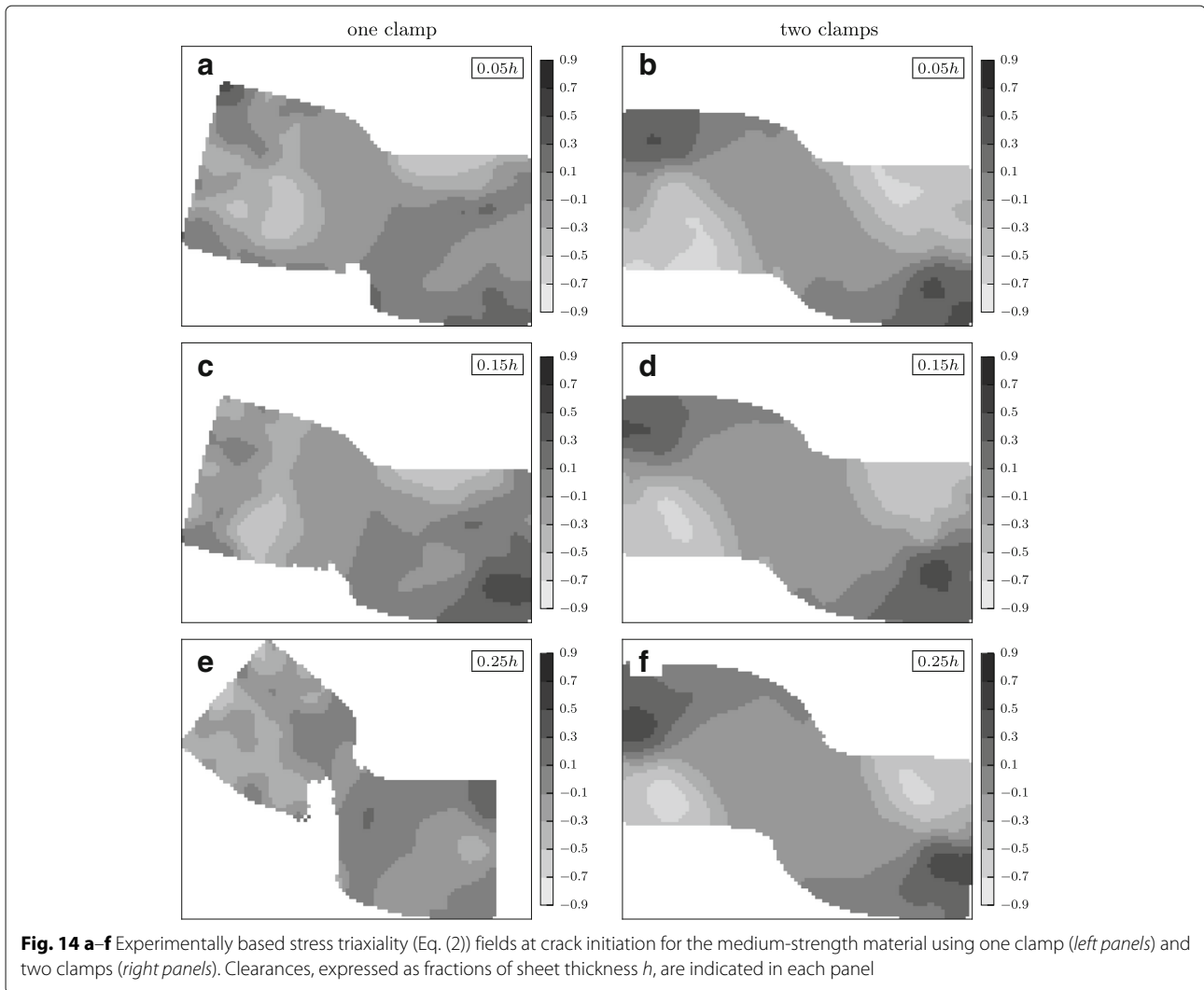




simulations for the bulk material and calculations from measurements for the surface, although not equal. For a correct comparison, either the simulations need to be in three dimensions and the triaxiality taken on the surface or the calculations from measured strains need to be done with the same plain strain approximation. A surface comparison would maybe be the most intuitive choice since strains are measured on the surface. On the other hand, the surface is a small part of the total shearing process, and therefore, the stress in the bulk material is of more interest. Consequently, in a strictly experimental aspect, the calculations from measured displacements should use the plane strain approximation to provide bulk material stresses. The present experimental results are still useful for validation of a three-dimensional finite element simulation.

The maximum strain was found in the sheet material around the curved tool profile. Within the zone that is plastically deformed, the maximum triaxiality was found in the material in contact with the vertical surface of the tool below the curved tool profile. Therefore, a larger impact of triaxiality on the crack initiation will result in a larger burr on the sheared samples.

Although gradients in the studied parameters are better resolved in the simulations compared with calculations from experiments, the result is still largely dependent on the mesh density. The gradients, and also the maximum value of the effective strain, will increase with smaller elements in contact with the tools and decrease with larger elements. Therefore, if the limitation in the digital image correlation technique close to the edges of the sheet is ignored, the mesh density in the finite element



simulations can be matched to the resolution in the measurements to obtain comparable results. This matching was initially done in the simulations, but the experimental results required filtering that reduced the effective resolution and the limitation in the measurements close to the edges was substantial. The measurements at the edges were also negatively influenced by the sample preparation as discussed by Gustafsson et al. (2016b). In the present state, the experiments are best used if the data close to the edges are ignored and the remaining data are used for validation of a finite element model that later can provide the missing experimental data.

A possible weak point in the present study is the identification of the point of crack initiation, which is the point during the shearing where all comparisons are made. The point of crack initiation was taken when the crack became visible on the surface in the captured images. Possibly, micro-cracks existed earlier, and the cracks on the surface

were maybe formed earlier or later than in the bulk material. A visible crack in a heavily sheared surface is quite subjective, and possibly, the tool displacement at crack initiation, that was also used in the FE simulations, was misinterpreted by a few tenth of a millimetre. Still, this would unlikely change the stress triaxiality to the magnitude that the observed spread would vanish or a clear trend become visible.

Conclusions

The stress and strain conditions at crack initiation in shearing of two steel sheet grades with various clearance and clamping were studied by calculations based on measured displacement fields and by finite element simulations. The finite element model was first validated against experimentally measured tool forces and strain fields on the sheet surface. Conclusions from the study were as follows:

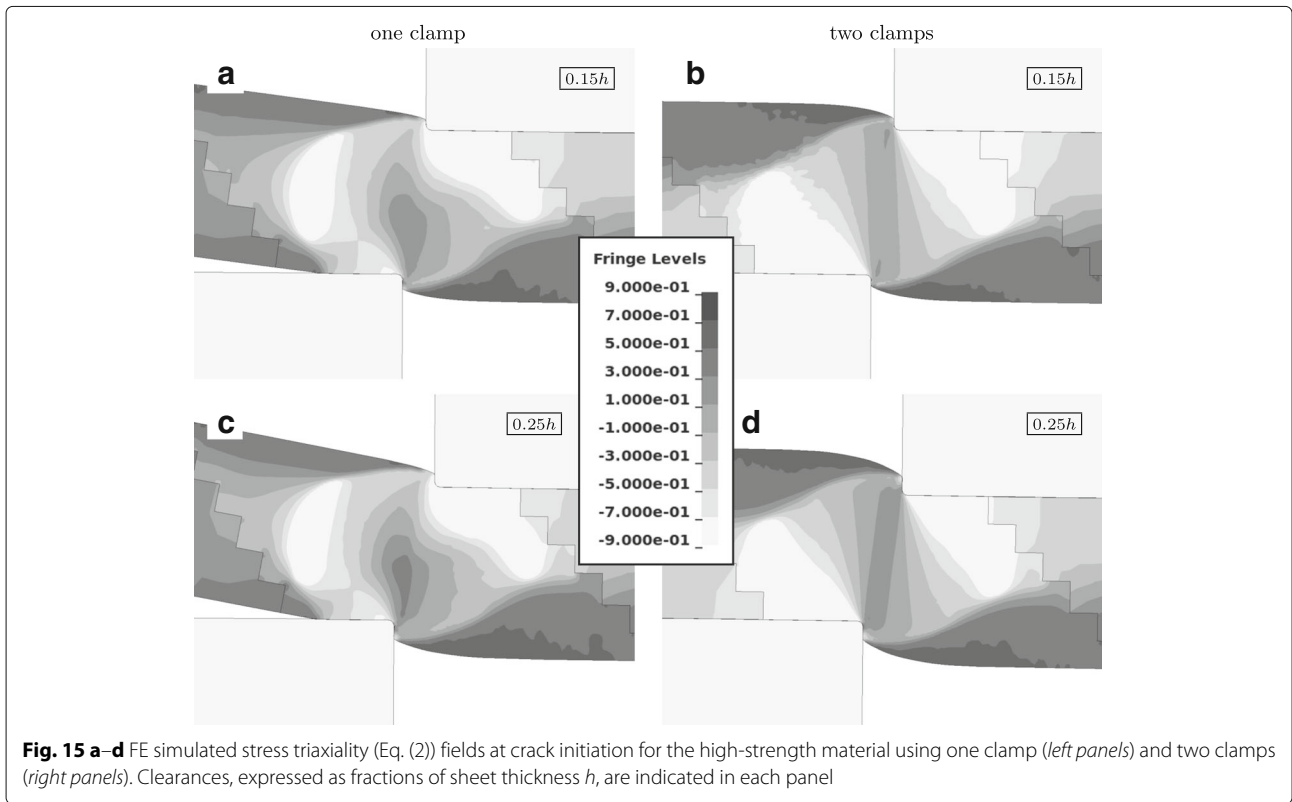


Fig. 15 a–d FE simulated stress triaxiality (Eq. (2)) fields at crack initiation for the high-strength material using one clamp (*left panels*) and two clamps (*right panels*). Clearances, expressed as fractions of sheet thickness h , are indicated in each panel

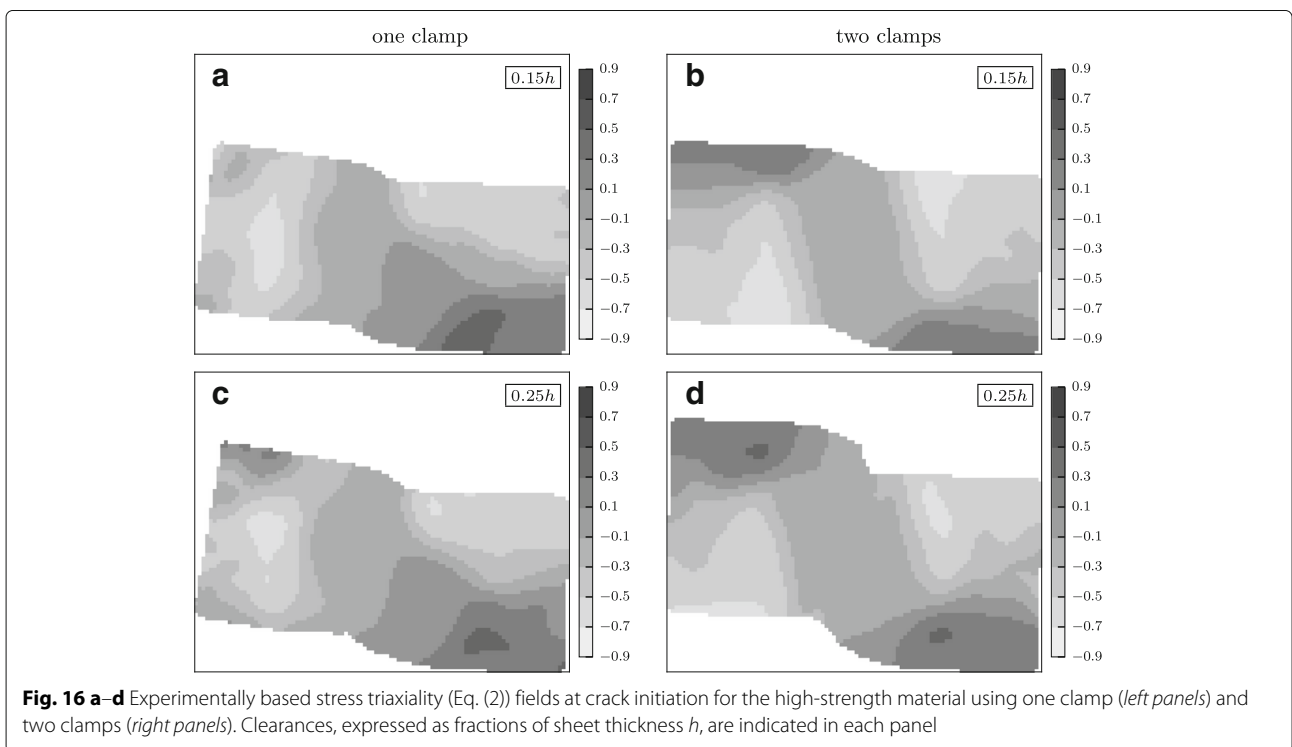


Fig. 16 a–d Experimentally based stress triaxiality (Eq. (2)) fields at crack initiation for the high-strength material using one clamp (*left panels*) and two clamps (*right panels*). Clearances, expressed as fractions of sheet thickness h , are indicated in each panel

Table 2 Summary of effective strains $\bar{\epsilon}$ (Eq. (3)), von Mises stresses $\bar{\sigma}$ [MPa] (Eq. (1)) and stress triaxiality η (Eq. (2)) at crack initiation for both experiments and simulations

	Medium strength						High strength			
	1 clamp			2 clamps			1 clamp		2 clamps	
	0.05h	0.15h	0.25h	0.05h	0.15h	0.25h	0.15h	0.25h	0.15h	0.25h
$\bar{\epsilon}_I^{\text{exp}}$	1.7	1.7	3.0	1.0	1.1	1.2	0.6	0.5	0.6	1.0
$\bar{\epsilon}_I^{\text{sim}}$	2.4	2.2	3.5	2.0	1.9	1.9	1.5	1.7	1.1	1.2
$\bar{\epsilon}_{II}^{\text{sim}}$	1.7	1.5	2.9	1.5	1.5	1.5	1.0	0.9	0.8	0.9
$\bar{\sigma}_I^{\text{exp}}$	850	840	870	820	820	840	1480	1480	1480	1480
$\bar{\sigma}_I^{\text{sim}}$	930	930	990	850	900	910	1520	1530	1530	1480
η_I^{exp}	0.2	0.05	0.2	0.1	0.1	0.1	0.2	0.2	0.05	0.1
η_I^{sim}	0.3	0.05	0.3	0.2	0.4	0.5	0.0	0.1	-0.2	0.3
η_{III}^{sim}	0.7	0.7	0.8	0.4	0.5	0.6	0.3	0.4	0.2	0.4

These parameters were evaluated in three regions denoted I, II and III and located as shown in Fig. (17). Steel sheets of two strength levels, two clamping configurations and three clearances, expressed as fractions of sheet thickness h , were used

- Effective strains and von Mises stresses were similar to the sheet surface and inside the bulk material. Mean stress, and therefore also triaxiality, was however not comparable on the surface and inside the material.
- There were large gradients in strain and stress around the curved tool profiles that were not captured by the experimental method. The results are still useful in combination with finite element simulations that are first validated with the

experimental data and later used to provide missing data of stress and strain at the sheet edges.

- Slightly larger effective strains and von Mises stresses were in general seen when shearing with one clamp compared with two clamps, but no clear trend was seen for the stress triaxialities.

Acknowledgements

This work was performed at Luleå University and at Dalarna University within the Swedish Steel Industry Graduate School, with financial support from Dalarna University (Högskolan Dalarna), Swedish Steel Producers' Association (Jernkontoret), County Administrative Board of Gävleborg (Länsstyrelsen i Gävleborg), Regional Development Council of Dalarna (Region Dalarna), Regional Development Council of Gävleborg (Region Gävleborg), Municipality of Sandviken (Sandvikens kommun) and SSAB.

Authors' contributions

EG conducted the experiments and FE simulations, collected the data and wrote the major part of the paper. SM calculated the stress from experimental measurements. MO and LK are EG's PhD supervisors, who guided and supported this work and contributed with their expertise and advices. All authors read and approved the final manuscript.

Competing interests

The authors declare that they have no competing interests.

Received: 3 January 2017 Accepted: 15 February 2017

Published online: 09 March 2017

References

- Cockcroft, MG, & Latham, DJ (1968). Ductility and the workability of metals. *Journal of the Institute of metals*, 96(1), 33–39.
- Gustafsson, E, Oldenburg, M, Jansson, A (2014). Design and validation of a sheet metal shearing experimental procedure. *Journal of Materials Processing Technology*, 214(11), 2468–2477.
- Gustafsson, E, Karlsson, L, Oldenburg, M (2016a). Experimental study of forces and energies during shearing of steel sheet with angled tools. *International Journal of Mechanical and Materials Engineering*, 11(1), 10.
- Gustafsson, E, Karlsson, L, Oldenburg, M (2016b). Experimental study of strain fields during shearing of medium- and high-strength steel sheet. *International Journal of Mechanical and Materials Engineering*, 11(1), 14.

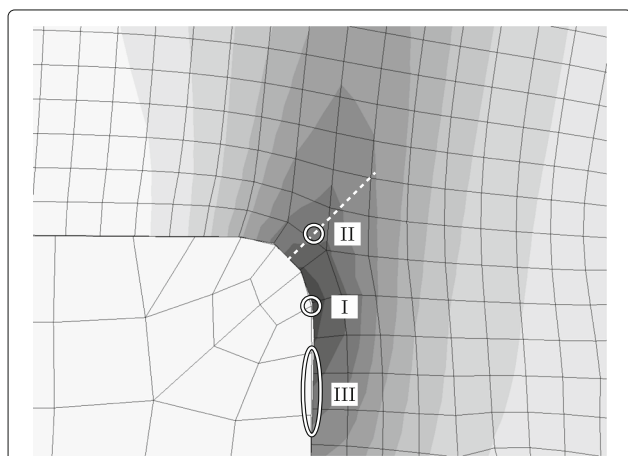


Fig. 17 Definition of locations, denoted I–III, close to the arc-shaped tool profile where the parameters in Table 2 were evaluated. *Point I*: transition from a vertical to an arc-shaped tool profile. *Point II*: 0.1 mm from middle of the arc profile along a direction 45° from the horizontal. *Region III*: close to the vertical tool profile just below point I. The image was taken from a simulation of shearing the medium-strength material with two clamps and 0.15h clearance. As length reference, the undeformed element size in the sheet mesh is 0.1 mm

- Hild, F, & Roux, S (2006). Digital image correlation: from displacement measurement to identification of elastic properties—a review. *Strain*, 42(2), 69–80.
- Hollomon, JH (1945). Tensile deformation. *Transactions of the American institute of mining and metallurgical engineers*, 162, 268–290.
- Johnson, GR, & Cook, WH (1985). Fracture characteristics of three metals subjected to various strains, strain rates, temperatures and pressures. *Engineering Fracture Mechanics*, 21(1), 31–48.
- Kajberg, J, & Lindkvist, G (2004). Characterisation of materials subjected to large strains by inverse modelling based on in-plane displacement fields. *International Journal of Solids and Structures*, 41(13), 3439–3459.
- Marth, S, Häggblad, HÅ, Oldenburg, M, Östlund, R (2016). Post necking characterisation for sheet metal materials using full field measurement. *Journal of Materials Processing Technology*, 238, 315–324.
- McClintock, FA (1968). A criterion for ductile fracture by the growth of holes. *Journal of Applied Mechanics*, 35(2), 363–371.
- Rice, J, & Tracey, D (1969). On the ductile enlargement of voids in triaxial stress fields. *Journal of the Mechanics and Physics of Solids*, 17(3), 201–217.
- Sjödahl, M (1994). Electronic speckle photography: increased accuracy by nonintegral pixel shifting. *Applied Optics*, 33(28), 6667–6673.
- Sjödahl, M (1997). Accuracy in electronic speckle photography. *Applied Optics*, 36(13), 2875–2885.
- Stegeman, Y, Goijaerts, A, Brokken, D, Brekelmans, W, Govaert, L, Baaijens, F (1999). An experimental and numerical study of a planar blanking process. *Journal of Materials Processing Technology*, 87, 266–276.

Submit your manuscript to a SpringerOpen[®] journal and benefit from:

- Convenient online submission
- Rigorous peer review
- Immediate publication on acceptance
- Open access: articles freely available online
- High visibility within the field
- Retaining the copyright to your article

Submit your next manuscript at ► springeropen.com
